UC Davis
UC Davis Previously Published Works

Title

A novel Bruch's membrane-mimetic electrospun substrate scaffold for human retinal pigment epithelium cells

Permalink

https://escholarship.org/uc/item/8dc2g1qj

Journal

Biomaterials, 35(37)

ISSN

0267-6605

Authors

Xiang, Ping
Wu, Kun-Chao
Zhu, Ying
et al.

Publication Date

2014-12-01

DOI

10.1016/j.biomaterials.2014.08.040

Peer reviewed

A novel Bruch's membrane-mimetic electrospun substrate scaffold for human retinal pigment epithelium cells

CrossMark

Ping Xiang [a], [1], Kun-Chao Wu [a], [1], Ying Zhu [b], Lue Xiang [a], Chong Li [c], Deng-Long Chen [b], Feng Chen [a], Guotong Xu [c], Aijun Wang [d], Min Li [b], [**], Zi-Bing Jin [a], [*]

[a] Laboratory for Stem Cell & Retinal Regeneration, The Eye Hospital of Wenzhou Medical University, Wenzhou 325027, China
[b] College of Life Science, Fujian Normal University, Fuzhou 350108, China
[c] Tongji Eye Institute, Tongji University School of Medicine, Shanghai 200092, China
[d] Surgical Bioengineering Laboratory, University of California Davis School of Medicine, CA 95817, USA

ARTICLE INFO

ABSTRACT

Various artificial membranes have been used as scaffolds for retinal pigment epithelium cells (RPE) for monolayer reconstruction, however, long-term cell viability and functionality are still largely unknown. This study aimed to construct an ultrathin porous nanofibrous film to mimic Bruch's membrane, and in particular to investigate human RPE cell responses to the resultant substrates. An ultrathin porous nanofibrous membrane was fabricated by using regenerated wild Antheraea pernyi silk fibroin (RWSF), polycaprolactone (PCL) and gelatin (Gt) and displayed a thickness of 3—5 μm, with a high porosity and an average fiber diameter of 166 ± 85 nm. Human RPE cells seeded on the RWSF/PCL/Gt membranes showed a higher cell growth rate ($p < 0.05$), and a typical expression pattern of RPE signature genes, with reduced expression of inflammatory mediators. With long-term cultivation on the substrates, RPE cells exhibited characteristic polygonal morphology and development of apical microvilli. Immunocytochemisty demonstrated RPE-specific expression profiles in cells after 12-weeks of co-culture on RWSF/PCL/Gt membranes. Interestingly, the cells on the RWSF/PCL/Gt membranes functionally secreted polarized PEDF and phagocytosed labeled porcine POS. Furthermore, RWSF/PCL/Gt membranes transplanted subsclerally exhibited excellent biocompatibility without any evidence of inflammation or rejection. In conclusion, we established a novel RWSF-based substrate for growth of RPE cells with excellent cyto-compatibility in vitro and biocompatibility in vivo for potential use as a prosthetic Bruch's membrane for RPE transplantation.

1. Introduction

Retinal pigment epithelium (RPE) is anatomically adjacent to the neurosensory retina, which is essential for vision creation and processing. The RPE is composed of a monolayer of polarized pigment cells, which lie on Bruch's membrane (BM). This epithelium plays a crucial role in a number of processes. These include: nourishment of the retinal visual cells; response to distinct extracellular signals; stray light absorption; retinal isomerization during the visual cycle; secretion of neurotrophic factors; phagocytosis of photoreceptor outer segments (POS); and preservation of the blood-retina barrier through tight junctions [1—5]. BM is a unique tissue with a thickness of 2—4 μm that serves as a molecular sieve to partially regulate the reciprocal exchange of nutrients, fluids, oxygen, and metabolic waste between the outer retina and the choroidal blood supply. It also acts as support for intact and functional cell sheet formation [6]. RPE dysfunction or cell loss is one of the major pathological changes leading to a wide range of retinal degenerative diseases, such as age-related macular degeneration (AMD) and some forms of retinitis pigmentosa (RP), which are the leading cause of blindness worldwide. Unfortunately, there is still no radical treatment to alleviate the progression of, or to recover the lost vision associated with, these diseases.

RPE cell replacement therapy is one of the most promising strategies to replenish or to replace RPE that has been damaged or lost [7—12]. Several studies have shown encouraging results with the injection of RPE cell suspensions in rodent models of retinal degeneration [13,14]. Subretinal transplantation of suspended RPE

* Corresponding author. Tel./fax: +86 577 88067926.
** Corresponding author. Tel./fax: +86 591 22867555.
E-mail addresses: mli@fjnu.edu.cn (M. Li), jinzb@mail.eye.ac.cn (Z.-B. Jin).
[1] These authors contributed equally.

cells in patients with AMD have been performed by many groups; however, the outcome has not been consistent [15–17]. Although subretinal transplantation shows promise, the subretinal injection of suspended RPE cells can potentially result in disorganized or misplaced grafts, as well as a reflux of cells from the injection site, which might lead to serious complications including RPE cell stacking, cell death, and retinal fibrosis.

Given that BM plays an essential role to maintain and support the physiological function of the RPE, it has been proposed that RPE cells can be seeded on a biodegradable and biocompatible prosthetic BM for use in cell transplants. A variety of thin and biodegradable polymer films including collagen [18–20], bombyx mori silk fibroin [21], polyimide [22], poly(hydroxybutyrate-co-hydroxyvalerate) [23], poly(d,l-lactic-glycolic acid) [24] and polyurethanes (PU) [25] have been employed for this purpose. However, it is currently unknown whether these prosthetic BMs can support the normal function of RPE cells and, most importantly, whether they elicit an inflammatory reaction after long-term co-culture.

Among the numerous fabrication techniques, electrospinning has become an exciting tool to generate nanofibrous network topographies that facilitate cell adhesion, proliferation and differentiation, as they allow for an efficient exchange of nutrients and metabolites across the nanofibers [26,27], and can also serve to deliver biochemical signals to the seeded cells [28,29]. Recently, electrospun nanofibers designed to bio-mimic the natural basement membranes used for retinal tissue engineering have received considerable attention [30]. PCL, a biodegradable aliphatic polyester with high tensile and elongation properties, has been widely used for tissue engineering applications [31–33] because it was approved by the U.S. Food and Drug Administration (FDA) for specific applications used in the human body [34]. Electrospun PCL nanofibers were demonstrated not only to support the growth and proliferation of retinal cells, but also showed biocompatibility after subretinal transplantation in an animal model [35,36]. However, inadequate cell affinity due to lack of recognition sites for cell adhesion and its inherent hydrophobicity make it less ideal for use as prosthetic Bruch's membrane material.

In our previous studies, recombinant spider silk protein (pNSR16, pNSR32) containing the Arg-Gly-Asp (RGD) cellular recognition sequences significantly enhanced cell adhesion and proliferation when blended with PCL [35] and other synthetic polymers [37]. Additionally, the addition of gelatin (10%, wt), which increased the hydrophilicity of scaffolds (PCL/pNSR32/Gelatin, 85:5:10, wt%), resulted in improved cell proliferation and cytocompatibility [12]. Wild *Antheraea pernyi* silk fibroin (RWSF) is a novel silk fibroin that has been studied extensively due to its extraordinary biocompatibility properties and reduced production costs. Our group and others have demonstrated RWSF could remarkably promote mammalian cell adhesion and proliferation when it was blended with synthetic materials due to its abundant RGD tripeptide motifs [38–40].

In this study, we fabricated by electrospinning an ultrathin and porous nanofibrous membrane composed of regenerated wild *Antheraea pernyi* silk fibroin (RWSF), PCL, and gelatin, to replicate the BM, and we investigated the biomaterial properties. Human RPE cells seeded on the electrospun membranes were evaluated following long-term (up to 12 weeks) co-culture and implanted into the eye of chinchilla rabbits. These novel RWSF-based substrates demonstrated cytocompatibility with human RPE cells, suggesting that these electrospun membranes could act as a potential prosthetic BM for RPE transplantation.

2. Materials and methods

2.1. Materials

Polycaprolactone (PCL) was purchased from Daicel Chemical Industries, Ltd, Japan. Gelatin (Gt) and 98wt% formic acid were purchased from Sinopharm Chemical Reagent Co., Ltd (Shanghai, China). Wild *Antheraea pernyi* silk was bought from Liaoning Tussah Silk Institute Co., Ltd. (Liaoning, China). Cell culture related reagents were obtained from Life Technologies Inc. (USA). Culture-grade plastics were purchased from Becton Dickinson Inc. (USA). Dimethyl sulfoxide (DMSO) was obtained from Sigma–Aldrich, Inc. (MO, USA).

2.2. Primary human RPE cells

Human adult posterior eye cups were obtained from Wenzhou Eye Bank with ethics committee approval and donor informed consent. RPE cells were isolated following a modified procedure, which was previously reported by Sonoda et al. [41]. Briefly, the eye tissue was placed in HBSS (Life Technology, USA) supplemented with 5% (vol/vol) penicillin-streptomycin for 20 min. Subsequently, the eye cup was dissected into four quadrants in order to lay flat followed by removal of the neural retina. The RPE-choroid sheets were carefully removed and digested in 2 mg/mL dispase (Roche, USA) dissolved in HBSS for 30 min in a CO_2 incubator. After digestion, the RPE layers were gently peeled off from the choroid, and then moved to a sterile culture dish, cut into small pieces in 0.05% trypsin-EDTA and digested for 20 min. The post-digestion solution containing RPE pieces was filtered using a 70 μm cell strainer (BD Biosciences, USA). The small RPE tissue clumps remaining on the apical side of the cell strainer were collected and placed into a T75 flask coated with 10 μg/mL Natural Mouse Laminin (Life Technologies Corporation, USA). RPE cells were fed with the addition of 2 mL hRPE media (High glucose DMEM with 15% FBS, 1% MEM Non-Essential Amino Acids Solution, 1 mg/mL GlutaMAX™ and 1% Antibiotic-Antimycotic Solution). After dissociation, RPE clumps adhered to the flask and migrated on the flask surface.

2.3. Electrospinning of ultrathin porous membranes

Regenerated wild *Antheraea pernyi* silk fibroin (RWSF) was prepared as described previously [40]. The polymer solutions with a concentration of 25% (wt/v) were prepared by dissolving RWSF, PCL and Gt with a weight ratio of 0:100:0 (PCL), 5:95:0 (RWSF/PCL), or 5:85:10 (RWSF/PCL/Gt) respectively in 98% formic acid. The electrospinning apparatus employed in this study contains a syringe pump (Baoding Longer Precision Pump Co., Ltd. Baoding, China), a high voltage supply (Tianjin Dongwen High Voltage Power Supply Co., Ltd., China), and a collector covered with aluminum foil. A voltage of 18 kV was applied to a syringe tip, while the collector was grounded. The polymer solution was loaded into a 5 mL disposable syringe with a blunt-end needle (0.6 mm internal diameter), which was controlled by a syringe pump at a feeding rate of 1.5 mL/h. The distance between needle tip and collector was adjusted to 15 cm. A charged jet of the solution was formed and ejected towards the collector, during which time the solvent evaporated and the fibers were deposited on the surface of the collector to form a flat nanofibrous membrane. The thickness of the electrospun membrane (EM) was controlled through the length of the processing time. All electrospinning experiments were performed at a constant temperature (40 ± 1 °C) and a relative humidity of 20 ± 5%. The as-spun nanofibers were dried in a fume cupboard at room temperature.

2.4. Characterization of electrospun Bruch's-mimetic membrane

Established membranes were subjected to an examination of their physicochemical properties including physical morphology, porosity, and wettability. To investigate the morphology, an electrospun ultrathin nanofibrous membrane was sputter coated with gold and observed using scanning electron microscopy (SEM; Model S-3000N, Hitachi, Japan). Images were captured using a SEM operating at an accelerating voltage of 15 kV with a 22 mm working distance. Image J software (NIH, USA) was used to calculate the mean and standard deviation (SD) of the fibers' diameters and by measuring thirty random fibers per image. Mean and SD of pore size were also obtained by approximation of surface pores from 30 measurements per image. In order to measure the porosity, membranes were dried in an electric blast drying oven for 2 h at 25 °C. Subsequently, they were put into a pycnometer full of degassed alcohol. The membranes were taken out, and the pycnometer and the remaining alcohol were weighed. The porosity of the membranes was calculated using the equations described below: The porosity $= (W_2 - W_3 - W_S)/(W_1 - W_3)$. Where W_1 is the weight of pycnometer that is filled with alcohol, W_2 refers to the weight of pycnometer with alcohol and scaffolds, W_3 to the weight of pycnometer and alcohol after removal of the scaffolds, and W_S is the initial weight of the membranes in a dry state. The wettability of electrospun membrane was evaluated in the light of water surface contact angle by a sessile drop method using 1 μL deionized water that was dropped onto the surfaces of nanofibrous membranes. After 10 s, the shapes of the water droplets were recorded by an optical contact angle meter system (OCA20, Dataphysics Instruments GmbH, Germany). Each determination was duplicated in five times in different positions. The values of contact angle were expressed as the mean ± SD.

2.5. Generation of human RPE cells and electrospun membrane (hRPE-EM) complex

ARPE-19, a human retinal pigment epithelium cell line, was routinely cultured in RPE medium (DMEM/F12 with 10% fetal bovine serum (FBS) and 1% penicillin-streptomycin). The EM were soaked in 75% ethanol for 24 h followed by washing three times with sterilized hanks balanced salt solution (HBSS). 1 mL DMEM/F12 (without FBS) was added into each well of a 24-well or 96-well plate and incubated

in 5% CO_2 at 37 °C for 24 h. ARPE-19 cells were seeded at a density of 4×10^5 cells/mL. RPE medium were carefully added onto the surface of membranes. For cell adhesion evaluation, the medium was aspirated and the material washed twice with HBSS to dislodge unbound or loosely adherent cells after 4 h incubation. Cell adhesion was observed by EVOS® xl core cell culture microscope (Advanced Microscopy Group, USA). For long-term studies, cells were grown for two weeks in RPE medium. After reaching confluence, the medium was replaced by DLP medium (DMEM with 1 g/L glucose, 1% FBS and 1 mM pyruvate) [42], then maintained for more than 12 weeks. DLP medium was changed twice a week.

2.6. Characterization of hRPE cell response to EMs

To investigate cell proliferation, hRPE-EM complexes were incubated for 1, 3, 5 and 7 days respectively. Tissue culture polystyrene (TCP) served as control. Cell proliferation was assessed using cellular metabolic activity and quantified using the Cell Proliferation Reagent WST-1 (Roche, Germany) according to the manufacturer's instructions. Briefly, 10 μL WST-1 reagent were added to each well, and then incubated for 4 h at 37 °C and 5% CO_2 to form formazan. The formazan concentration was measured by absorbance at 440 nm using a Multi-Detection Microplate Reader (Spectra Max M5/M5e, Molecular Devices, USA).

To test whether the EMs altered the cell cycle, we performed cell cycle analysis. Cells were harvested by 0.05% Trypsin-EDTA digestion from the hRPE-EM complexes and were fixed in pre-cooling 70% ethanol overnight. Fixed cells were treated using Cell Cycle and Apoptosis Analysis Kit (Beyotime Institute of Biotechnology, China) according to the manufacturer's manual. The total number of cells in different phases of the cell cycle was detected using flow cytometry (Cytomics™ FC500 Flow Cytometry, Beckman Coulter Ltd., USA).

2.7. Gene expression profiling of hRPE-EM complexes

Total RNA was extracted using Trizol reagent (Life Technologies, USA), according to the manufacturer's instructions and RNase-Free DNase I (Beyotime Institute of Biotechnology, China) was used to remove contaminating DNA. The quality of RNA was measured using a NanoDrop ND-1000 Spectrophotometer (Thermo Fisher Scientific Inc., USA). cDNA synthesis was conducted using AMV Reverse Transcriptase (Promega Corporation, USA). Reverse transcription polymerase chain reactions (RT-PCRs) were performed using specific primers (Table 1) to analyze the expression levels of RPE-marker genes and pro-inflammatory genes. PCR products were analyzed on 2% agarose gels and visualized using the Gel Imaging System (BIO-RAD ChemiDocXRS, USA).

2.8. Measurement of physiological functions of RPE-EM complex

Because RPE cells have essential functions in vivo including polarized neurotrophin secretion and phagocytosis, we examined the functionality of the RPE cells in the RPE-EM complex. RPE-EM complexes were placed on the bottom of apical chambers of 6.5-mm uncoated Transwell polyester filters (Corning Inc., USA) after 4 weeks of culture. Media from the apical and basal chambers were collected respectively for 24 h after the last change of media. Secretion of pigment epithelium derived factor (PEDF) was measured using the human PEDF enzyme-linked immunosorbent assay (ELISA) kit (Cusabio, China) according to the manufacturer's instructions.

To test the ability of the EM-combined RPE cell of phagocytosis, fresh porcine eyes were collected and photoreceptor outer segments (POS) were isolated and conjugated with FITC (Life Technologies, USA), as previously described [43]. ARPE-19 cells were seeded on RWSF/PCL/Gt membranes, maintained in DLP medium for 4 weeks, and then incubated with FITC-covalent POS for 4 h in the CO_2 incubator. To exclude false positive staining caused by external binding of FITC-POS, cultures were washed 4 times with PBS, followed treatment with 0.2% trypan blue for 10 min. Cells were then fixed with 4% paraformaldehyde and counterstained with DAPI to label nuclei. The stained cells were imaged with a fluorescence microscope (Carl Zeiss

Meditec, Inc., Germany) in 5 random areas. Phagocytic activities were calculated using the following equation: Phagocytic activity = Number of FITC (green) labeled particles/Number of nuclei.

The micro-morphology of the cells seeded on RWSF/PCL/Gt membranes was evaluated using scanning electron microscopy (SEM). In brief, RPE-EM complexes were collected after 4 weeks cultivation, washed with HBSS twice and then fixed with 2.5% glutaraldehyde for 2 h. Cell-membrane complexes were dehydrated through a series of graded ethanol solutions, followed by CO_2 critical point drying before sputter coating with gold and then subjected to SEM.

2.9. Immunohistochemistry

RPE cells cultured on RWSF/PCL/Gt membranes were washed three times with PBS, fixed in freshly prepared 4% paraformaldehyde for 20 min, permeabilized with 0.1% Triton X-100 in PBS for 30 min. After blocking for 1 h with 5% normal goat serum in PBS with 0.1% Tween-20 (PBST), cells were stained with the following primary antibodies: ZO-1 (1:200; Invitrogen), MITF (1:500; Millipore), PEDF (1:250; Millipore) and RPE65 (1:250; Millipore) overnight at 4 °C. Cells were washed and incubated with the following secondary antibodies: TRITC/FITC-conjugated goat anti-mouse IgG (1:200; Jackson ImmunoResearch Laboratories, Inc.) and TRITC/FITC-conjugated goat anti-rabit IgG (1:200; Jackson ImmunoResearch Laboratories, Inc.) for 1 h at 37 °C. Cell nuclei were counterstained using DAPI. Cells were visualized using a fluorescence microscope (Carl Zeiss Meditec, Inc., Germany).

2.10. RNA sequencing of human primary RPE cells on the RWSF/PCL/Gt

Total RNA was extracted from cultured primary RPE cells and the same cells grown on EM as described above. RNA quality was assessed using capillary gel electrophoresis with a Bioanalyser 2100 (RNA nano kits, Agilent). mRNA-Seq libraries were generated from total RNA with polyA+ selection of mRNA using the TruSeq RNA Sample Prep Kit v2 (Illumina, San Diego, CA), and then subjected to transcriptome sequencing on the Illumina Hiseq 2000. Short sequence reads were generated, and after filtering reads containing sequencing adapters and low quality, the remaining reads were aligned to the human reference genome (hg19; UCSC, http://genome.ucsc.edu) using Bowtie, allowing up to 2 base mismatches. We then applied cufflinks to measure transcript abundances in Fragments Per Kilobase of exon per Million fragments mapped (FPKM) and identified the differentially expressed genes (DEG). Furthermore, the gene ontology (GO) and KEGG pathway enrichment analyses on the DEGs were performed on DAVID (http://david.abcc.ncifcrf.gov/).

2.11. Biocompatibility testing of RWSF/PCL/Gt by intraocular transplantation

Based on above results, RWSF/PCL/Gt substrate was chosen for the following short-term subretinal biocompatibility studies. All treatments were carried out in accordance with the ARVO Statment for the Use of Animals in Ophthalmic and Vision Research.

Briefly, 5 chinchilla rabbits at 2–2.5 kg were supplied by the animal center of Wenzhou Medical University. The EMs were cut into rectangles (3 mm × 2 mm) then soaked in 75% ethanol for 24 h followed by 3 washes in 0.1 M sterilized phosphate buffered saline (pH 7.2, PBS) for intraocular transplantation. Only the right eye was used for experimentation. One month after transplantation, rabbits were euthanized under deep anesthesia with an intramuscular injection of pentobarbital sodium. The rabbits' eyes were collected and fixed in 4% paraformaldehyde for 48 h. The anterior segments of the eye were removed and full thickness samples (retina/sclera) of the implantation site were excised and paraffin-embedded. The samples were then sectioned and stained with hematoxylin and eosin (HE) as described previously [44].

Table 1
Primers used for Reverse transcription PCR (RT-PCR).

Gene	Forward primer (5′–3′)	Reserve primer (5′–3′)	Accession no.	Tm (°C)
MITF	AAGTCCTGAGCTTGCCATGT	GGCAGACCT TGGTTTCCAA	NM_001184968.1	52
PMEL17	GTGGTCAGCACCCAGCTTAT	GAGGAGGGGGCTATTCTCAC	NM_006928	52
KRT8	AAGGATGCCAACGCCAAGTT	CCGCTGGTGGTCTTCGTATG	NM_002273	60
CNTF	GGGATGGCTTTCACAGAGCA	GCCCTGATGCTTCACATAGGAT	NM_000614.3	57
VEGF	CTCCACCATGCCAAGTGGTC	GCAGTAGCTGCGCTGATAGA	NM_001204385.1	55
PEDF	TTACGAAGGCGAAGTCACCA	TAAGGTGATAGTCCAGCGGG	NM_002615.5	58
CRALBP	GCTGCTGGAGAATGAGGAAACT	TGAACCGGGCTGGGAAGGAATC	NM_000326.4	61
Na+/K+ ATPase	AATTCGGTCTTCCAGCAGGG	ACCAGGTAGGTTTGAGGGGA	NM_001160234.1	60
IL-1β	TTACAGTGGCAATGAGGATGAC	TGTAGTGGTGGTCGGAGATTC	NM_000576.2	58
MCP-1	GCTCATAGCAGCCACCTTCAT	TCACAGCTTCTTTGGGACACTT	NM_002982.3	54
IL-6	CAATCTGGATTCAATGAGGAGAC	CTCTGGCTTGTTCCTCACTACTC	NM_000600.3	60
β-actin	TCCCTGGAGAAGAGCTACGA	AGGAAGGAAGGCTGGAAGAG	NM_001101.3	60
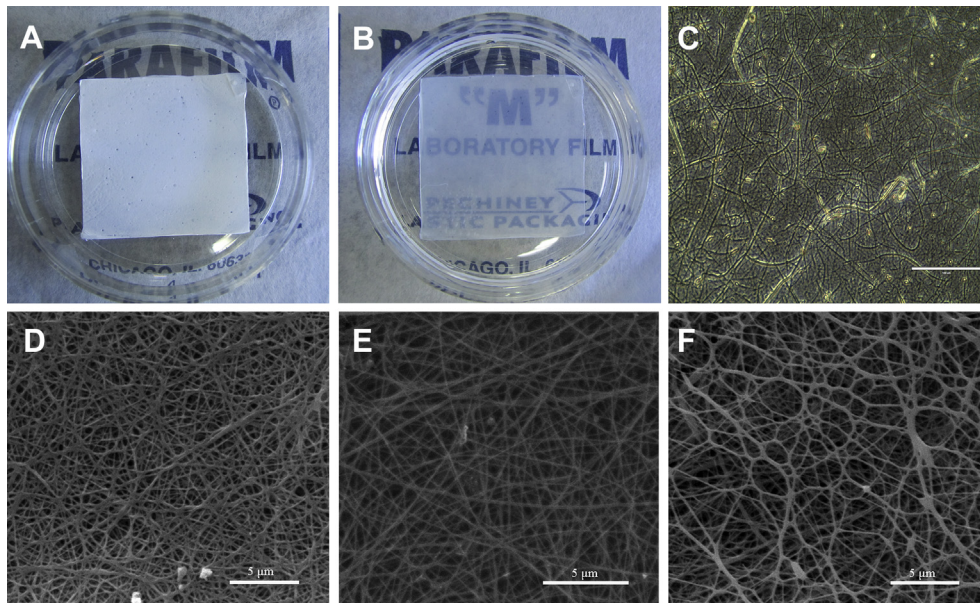
Fig. 1. Appearance of electrospun membranes before (A) and after (B) immersion in 75% ethanol and (C) phase contrast image following treatment with PBS. SEM micrographs of (D) PCL, (E) PCL/RWSF, (F) PCL/RWSF/Gt Scale bar = 100 μm.

2.12. Statistical analysis

Results are presented as mean ± SD. Statistical analyses were performed using ANOVA by PASW Statistics Version 18 (SPSS Inc., USA) and Graphpad Prism Version 5 (Graphpad Software, USA). Differences were considered statistically significant if the p value was less than 0.05.

3. Results

3.1. Physicochemical property of the nanofibrous membranes

In this study, ultrathin membranes (thicknesses were approximately 3–5 μm) composed of PCL, RWSF and Gt were successfully produced by electrospinning (Fig. 1). Intriguingly, the resultant membranes demonstrated transparency following immersion in ethanol or cell culture media (Fig. 1B), thus cell growth on the electrospun membranes could be observed directly. SEM images depicting the micromorphology of the electrospun nanofibrous membranes are shown in Fig. 1D–F, including images of electrospun RWSF/PCL/Gt membranes (Fig. 1F) and PCL and RWSF/PCL control membranes (Fig. 1 D, E). All three types of membranes were constructed of randomly oriented fibers and thoroughly interconnected pore structures. However, membranes containing gelatin displayed significantly increased fiber diameter, pore diameter and porosity relative to PCL and RWSF/PCL (Table 2). The average fiber diameter of electrospun PCL (157 ± 56 nm) was similar to the electrospun RWSF/PCL (154 ± 61 nm), but both were much smaller in diameter than RWSF/PCL/Gt (253 ± 93 nm; $p < 0.05$). Additionally, electrospun RWSF/PCL/Gt demonstrated significantly larger pore diameter (2078 ± 1104 nm) than either PCL (681 ± 313 nm) or RWSF/PCL (1129 ± 457 nm; $p < 0.05$). The wettability of the membranes was determined by contact angle

analysis (Table 3 and Fig. S1). This analysis indicated that the hydrophilicity of RWSF/PCL/Gt was much higher than either that of PCL or RWSF/PCL, suggesting that the addition of Gt strikingly improved the hydrophilicity.

3.2. Cell adhesion to the EMs

To assess cell adhesion, ARPE-19 cells growing on the nanofibrous membranes were analyzed using an inverted microscope. As shown in Fig. 2, cells were able to attach and spread on all materials. However, the shape of ARPE-19 on PCL (Fig. 2B) was rounded, indicating feeble cell adhesion. Importantly, the cell shapes have improved after seeding on RWSF/PCL and RWSF/PCL/Gt membranes because they are no longer round. Furthermore, the density of cells growing on the RWSF/PCL/Gt membranes (Fig. 2D) was similar to TCP (Fig. 2A), and much greater than that on either RWSF/PCL (Fig. 2C) or PCL (Fig. 2B) membranes. Therefore, the addition of RWSF and gelatin into the membrane composite significantly enhanced cell adhesion.

### 3.3. EMs-combined RPE cells showed high cell viability

WST-1 analysis was performed to observe cell viability and proliferation on the different electrospun membranes and TCP. As shown in Fig. 2E, the ARPE-19 cells were proliferative, and the density of cells increased with culture time on all of the various membranes as well as on TCP, indicating that the artificial membranes were supportive for human RPE cells proliferation. However, the proliferation rate of ARPE-19 cells on RWSF/PCL/Gt and RWSF/PCL was higher than on PCL ($p < 0.01$), and similar to the

Table 2
Porosity and pore size of electrospun membranes ($n = 30$).

Substrate	Fiber diameter (nm)	Porosity (%)	Pore diameter (nm)
PCL	157 ± 56	85.0 ± 2.6	681 ± 313
RWSF/PCL	154 ± 61	87.0 ± 1.7	1129 ± 457
RWSF/PCL/Gt	253 ± 93	90.6 ± 3.9	2078 ± 1104

Table 3
Contact angle of electrospun membranes ($n = 5$).

Substrate	Contact angle (°)
PCL	117.38 ± 9.67
RWSF/PCL	119.02 ± 6.47
RWSF/PCL/Gt	64.48 ± 4.93
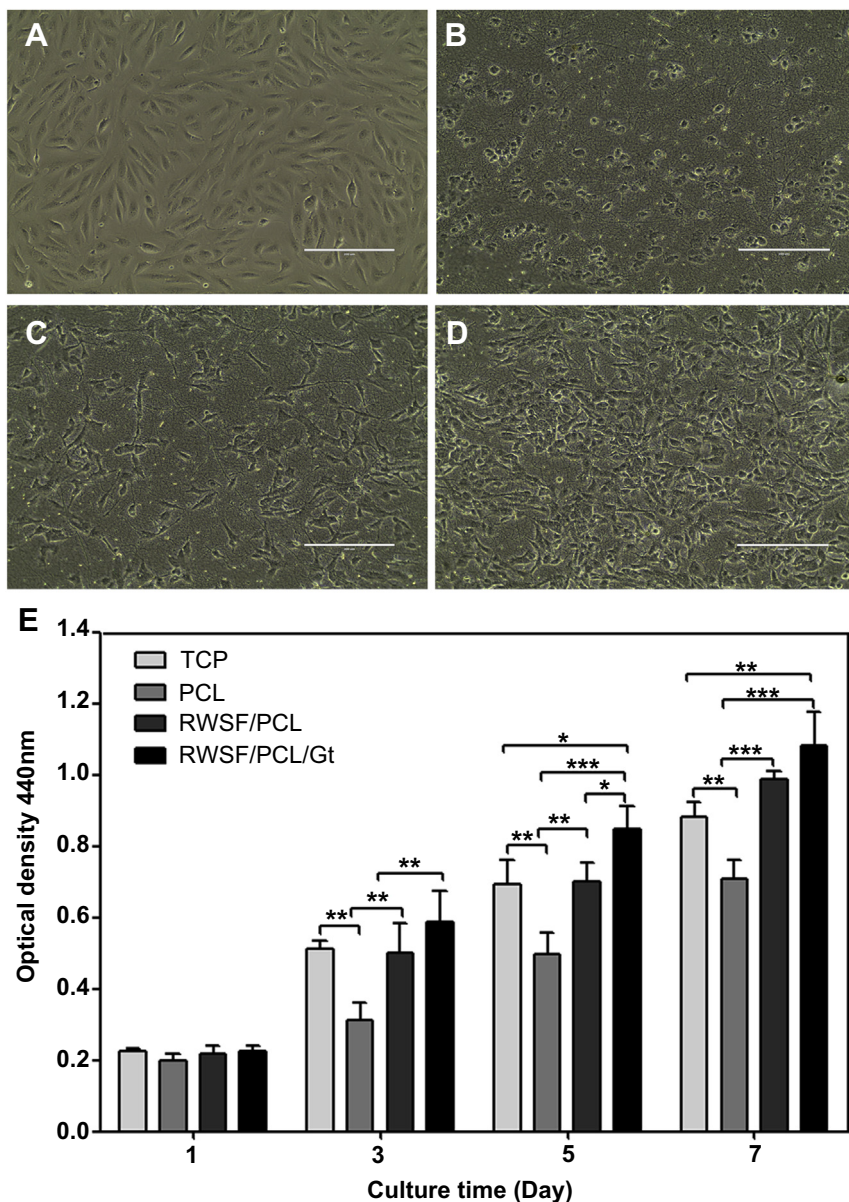
Fig. 2. ARPE-19 cultured on (A) TCP, (B) PCL, (C) PCL/RWSF, (D) PCL/RWSF/Gt membranes for 24 h and measurements of proliferation on various electrospun membranes for up to 7 days (E). Micrographs indicated that PCL/RWSF/Gt membranes induced greater cell densities than that on PCL and PCL/RWSF after 24 h of culture. ARPE-19 attached on all electrospun membranes at comparable densities on first day. Proliferation of ARPE-19 cells on PCL/RWSF/Gt and PCL/RWSF was higher than PCL, but similar to that on TCP on the third day. ARPE-19 cells on PCL/RWSF/Gt showed the fastest growth rate among all groups even compared with TCP on day 5 and day 7. Results were expressed as mean $\pm$ s.d. ($n = 5$), * means $P < 0.05$, ** means $P < 0.01$, *** means $P < 0.001$ (from WST-1 test).

level of proliferation on TCP on the third day. ARPE-19 cells showed the quickest rate of growth on RWSF/PCL/Gt amongst all of the nanofibrous membranes. The RWSF/PCL membrane promoted cell growth and spreading compared with PCL ($p < 0.01$) 5 days after seeding. Likewise, on the 7th day, the maximum amount of ARPE-19 cells was still observed on the RWSF/PCL/Gt. This result suggested that, in comparison to other electrospun membranes and TCP, the membrane blending of PCL with RWSF and Gt might accelerate cell growth and proliferation.

3.4. EMs do not alter cell cycle of the RPE cells

To compare cell growth on different substrates, we employed cell cycle analysis using proliferation indexes (PI) [(G2/M + S)/(G0/G1+G2/M + S), 100%] (Table 4 and Fig. 3). Interestingly, there were

remarkable differences observed among PCL and other substrates, including RWSF/PCL/Gt, RWSF/PCL and TCP. Approximately 29.3% of the cell population on RWSF/PCL/Gt membranes remained actively cycling (G2/M + S) while fewer cells on PCL (16.2%),

Table 4
Results of cell cycle analysis on various substrata.

Substrata	Cell cycle			
	G_0/G_1 (%)	S (%)	G_2/M (%)	PI (%)
TCP	77.60 ± 0.64	20.25 ± 4.03	2.11 ± 1.49	23.7
PCL	83.77 ± 1.15	15.37 ± 0.81	0.82 ± 0.38	16.2
RWSF/PCL	78.7 ± 1.82	19.13 ± 3.43	2.19 ± 1.57	21.3
RWSF/PCL/Gt	70.65 ± 0.35	25.30 ± 1.56	4.01 ± 1.19	29.3
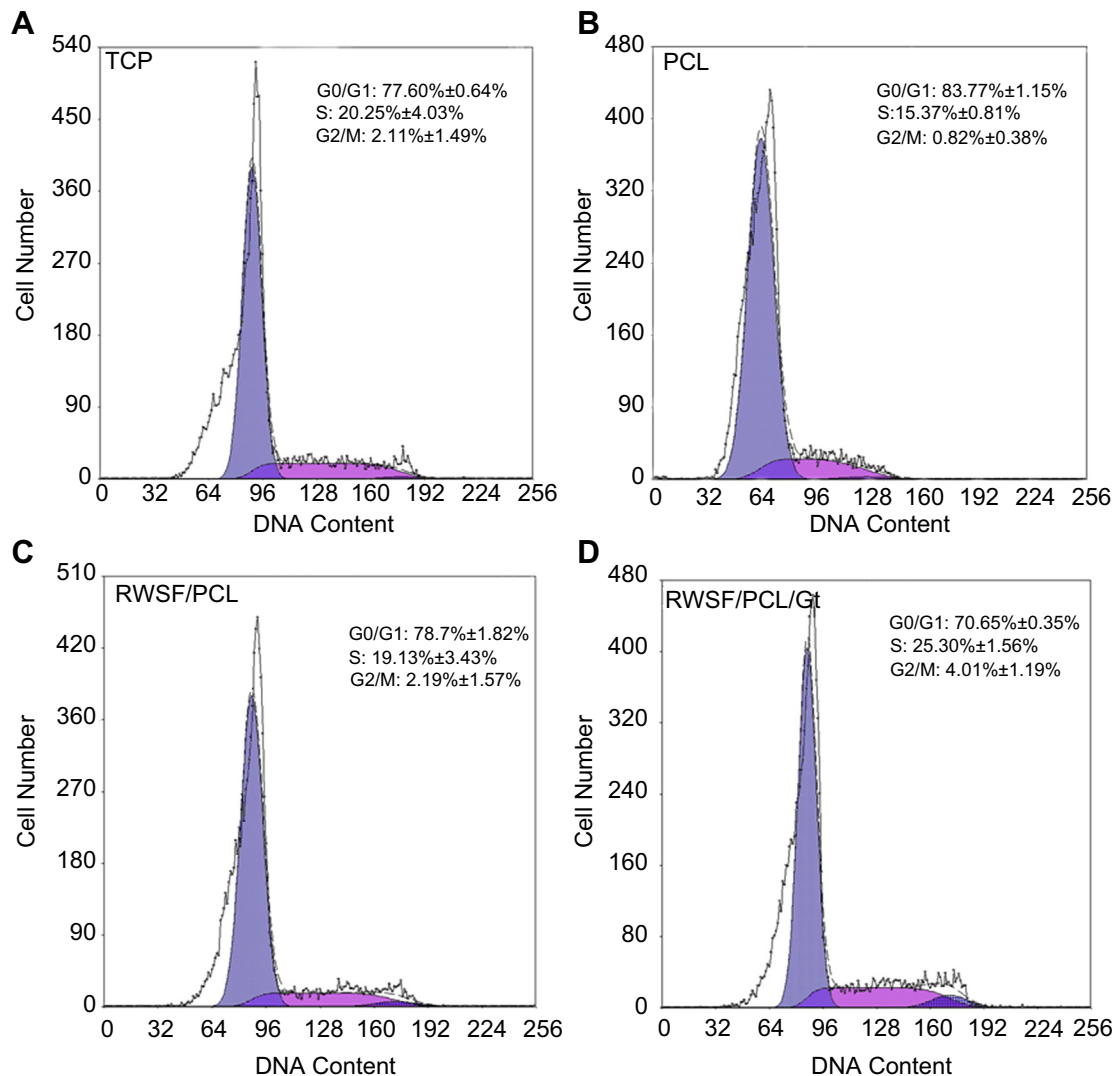
Fig. 3. Cell cycle analysis of ARPE-19 cells grown on various membranes after 3 days of culture. Approximately 29.3% of the cell population on PCL/RWSF/Gt (D) remained in active cycling (G2/M + S) while fewer cells on PCL (B) (16.2%), PCL/RWSF (C) (21.3%) and TCP (A) (23.7%) kept in kinetic phase.

RWSF/PCL (21.3%) and TCP (23.7%) kept the kinetic phase. These results suggest that RWSF/PCL/Gt membranes enhance cell proliferation, similarly to what observed for the WST-1 test above.

3.5. RPE cells grown on RWSF/PCL/Gt express marker genes

The transcriptional levels of RPE marker genes including *Na+/K+ ATPase*, *TYR*, *CRALBP*, *PEDF*, *CNTF*, *VEGF*, *KRT8*, *MITF* and *PMEL 17* were examined by RT-PCR and RNA sequencing after seeding on various electrospun membranes for 2 weeks. ARPE-19 on different electrospun membranes as well as on TCP exhibited similar transcriptional level of the marker genes (Fig. 4A).

3.6. RPE cells combined with RWSF/PCL/Gt elicited lower expression levels of inflammatory genes

It has been known that many biomaterials can elicit elevated expression of inflammatory genes. Using RT-PCR and transcriptome analysis, we demonstrated that RPE cells grown on RWSF/PCL/Gt exhibited the lowest levels of expression of inflammatory genes (Fig. 4B), suggesting that RWSF/PCL/Gt might not elicit obvious inflammatory responses.

3.7. Gene-expression signatures of RPE-EMs

To investigate the gene expression profiling, we performed RNA-sequencing. Both the primary RPE cells and the RPE-EMs showed significant expression of signature genes (Fig. 4C) as previously reported [45]. This result clearly demonstrated that RPE cells on the RWSF/PCL/Gt complex maintained the gene-expression signatures of primary RPE.

3.8. RPE complex displayed morphological and physiological features: pigmentation, microvilli, tight junction, phagocytic ability, and neurotrophin secretion

After long term co-culture with RWSF/PCL/Gt membrane, ARPE-19 developed into a confluent monolayer of cells demonstrating typical, tightly cobble-stone like or polygonal shape, and pigmentation (Fig. 5). Furthermore, the more polygonal areas exhibited apical distribution of projections with analogical features to microvilli (Fig. 6A–B) which is an indispensable structure of RPE cells *in vivo*.

The capacity for phagocytosis of photoreceptor outer segments (POS) is a pivotally physiological function of RPE cells, as
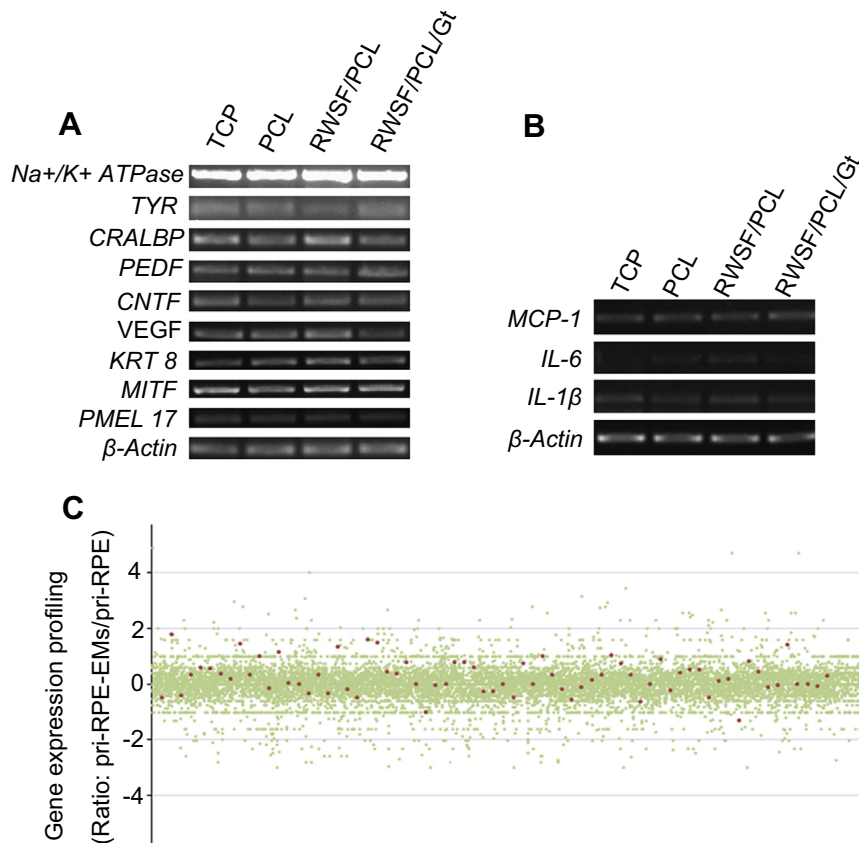
Fig. 4. Semi-quantitative RT-PCR detection of RPE cell signature genes and inflammatory factors after cultivation on various electrospun membranes for 24 h and 2 weeks, respectively. (A) Nine signature genes of RPE cells showed equivalent levels of expression when ARPE-19 cells were cultured on different membranes and TCP; (B) Based on RT-PCR analysis, cells grown on all electrospun membranes did not significantly increase the expression of *MCP-1*, *IL-1β* and *IL-6* compared to TCP. (C) The primary RPE cells on the EMs showed significantly similar gene expression profiling with the primary RPE cells. Green dots represent the ratio of gene expression, red dots indicate the ratio of RPE signature genes. pri-RPE, primary RPE. (For interpretation of the references to color in this figure legend, the reader is referred to the web version of this article.)

dysfunction leads to retinal degenerative diseases [46]. ARPE-19 cells were cultured both on TCP and RWSF/PCL/Gt for 4 weeks followed by incubation with FITC-conjugated porcine POS, as reported previously [47]. The phagocytic activity for ARPE-19 cells grown on RWSF/PCL/Gt membranes was 1.89 ± 0.33 and on TCP was 1.11 ± 0.19 (Fig. 6C, D). Thus, the phagocytic activity of ARPE-19 cells grown on RWSF/PCL/Gt membranes was approximately 1.7-fold higher than that on TCP.
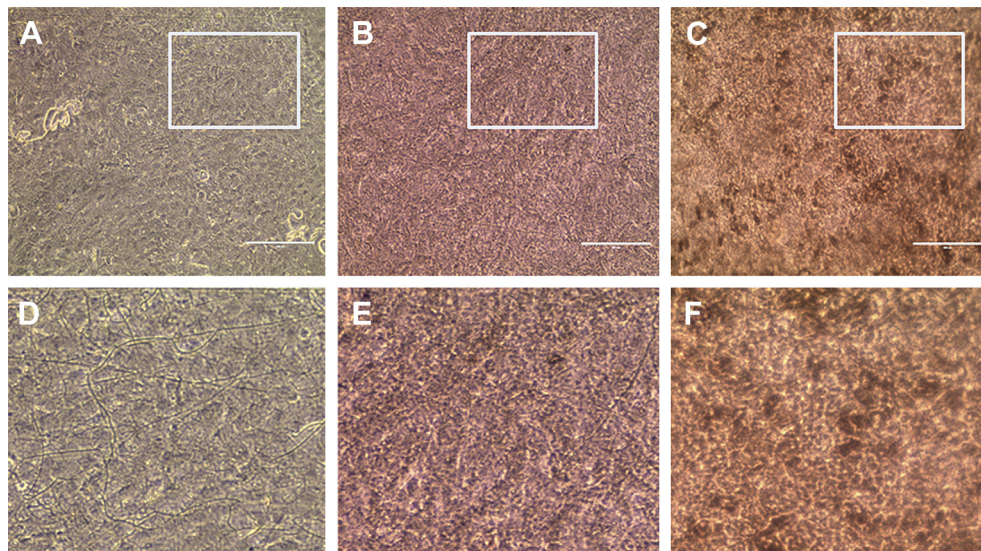
Fig. 5. Establishment of long-term cultures of ARPE-19 cells on RWSF/PCL/Gt membranes. (A, D) Appearance of typical culture of ARPE-19 cells on RWSF/PCL/Gt membranes after 30 days displaying the polygonal shape of the cells; (B, E) After 60 days culture, ARPE-19 cells exhibited much smaller volume and tighter junctions; (C, F) Melanin pigment appears in cells on RWSF/PCL/Gt membranes on day 90. D, E, F correspond to higher magnification images of the areas in the white rectangular boxes in A, B, C, respectively.
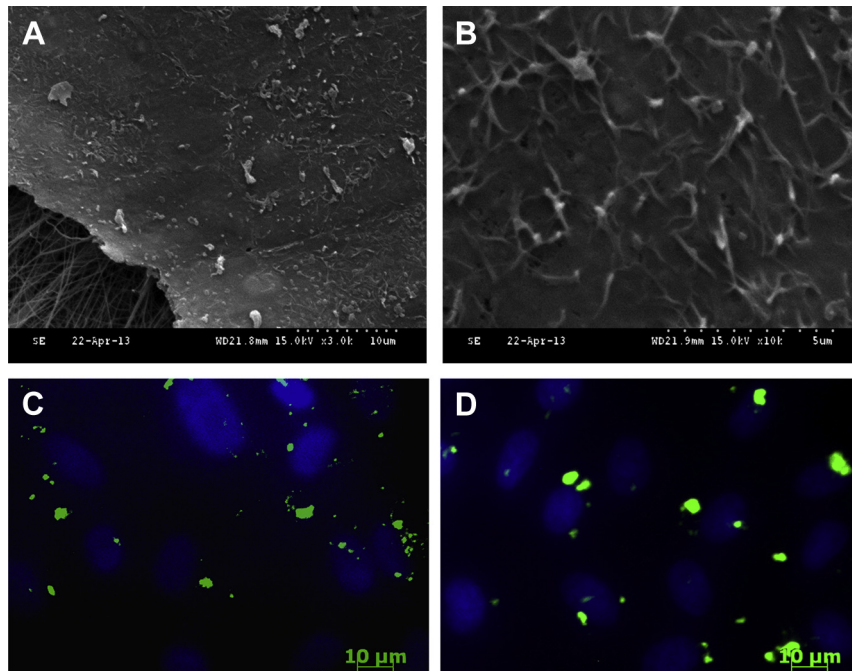
Fig. 6. RPE-EM complexes displayed tight junctions, microvilli formation and phagocytic ability. (A, B) Scanning electron microscope (SEM) images displayed ARPE-19 cells developed into typical polygonal morphology and formed tight junctions (A) and apical microvilli (B) [magnification: 3000 (A), 10,000 (B)] after 4 weeks cultivation on RWSF/PCL/Gt membranes. ARPE-19 cells cultured on RWSF/PCL/Gt membranes for 4 weeks showed higher phagocytic activity of FITC-conjugated porcine POS than that of cells grown on TCP (C–D). Blue and green indicate nuclei and phagocytosed POS, respectively. (For interpretation of the references to color in this figure legend, the reader is referred to the web version of this article.)

To test if growth on the membranes alters the polarized secretion of neurotrophins, ARPE-19 cells were grown in Transwells with or without electrospun membranes coated with cells for 4 weeks. PEDF was detected by ELISA in the culture medium harvested from both the upper and lower reservoirs. However, ARPE-19 cells cultured on RWSF/PCL/Gt and RWSF/PCL membranes demonstrated typically polarized secretion of PEDF (Fig. 7A); the apical side had a higher concentration of PEDF than the basolateral side. In contrast, polarized secretion of PEDF was not observed in ARPE-19 cells seeded on PCL membranes, suggesting the addition of RWSF/Gt promoted the polarized secretion of RPE cells *in vitro*. Together, these findings clearly suggest that RWSF/PCL/Gt membranes not only supported cells growth for a long period of time, but also promoted cell polarization and functionalization.

3.9. RPE-EMs expressed a group of markers

After long-term culture on electrospun membranes, ARPE-19 spread to a confluent monolayer and developed various differentiated features of RPE cells *in vivo* as confirmed by the *bona fide* expression pattern of several markers. ARPE-19 cells stained positively for ZO-1, MITF and DAPI after 8 weeks culture on electrospun RWSF/PCL/Gt membranes (Fig. 7B). DAPI staining showed a uniform distribution of nuclei, indicating monolayer construction without overlap. Positive expression of ZO-1 suggested that the ARPE-19 cells formed tight junctions (Fig. 7B). Moreover, MITF, a key regulator for RPE cell differentiation and proliferation, was observed (Fig. 7B). Encouragingly, after 12 weeks cultivation, both RPE65, a specific retinal pigmented epithelial cell enzyme essential for the visual cycle, and PEDF (Fig. 7B) were positively expressed in the RPE cells grown on the RWSF/PCL/Gt membrane. Collectively, these data demonstrated that complex RPE on RWSF/PCL/Gt membrane maintained its cell characteristics as *in vivo*.

### 3.10. EMs demonstrate biocompatibility in vivo

RWSF/PCL/Gt membranes were successfully implanted into the intraocular space (sub-sclera) in 5 eyes of 5 rabbits. Histological staining showed RWSF/PCL/Gt membranes to be well-tolerated in the intraocular space without inflammation in sclera or retina (Fig. 8), indicating that the membranes would be useful as a cell scaffold for transplantation.

4. Discussion

Accumulating evidence suggests that transplantation of a polarized and intact RPE cell monolayer, instead of injections of cell suspensions, might be more feasible for functional RPE reconstruction [48]. Many artificial carrier substrates, both natural and synthetic, have served as BM prosthesis to support the attachment and growth of RPE cells [49]. However, these artificial substrates still have disadvantages due to their incomparable ultrastructure, limited biodegradability and reduced ability to support RPE cells after long-term co-culture, as well as the possibility of eliciting adverse tissue response.

An ideal BM-mimetic would exhibit the following properties: a thickness of less than 5 μm; a porous ultrastructure to allow the transport of nutrients and metabolic waste; biocompatibility for cell adhesion and growth; maintenance of signature genes of RPE cell expression. Importantly, the BM-mimetic should also preserve the physiological RPE features *in vivo*, such as, polygonal shape and formation of tight junctions, phagocytosis of ROS, formation of apical microvilli, the polarized secretion of neurotrophic factors, and without inflammation after implantation.

In this study, PCL, RWSF, and gelatin were chosen to prepare the Bruch's membrane-mimetic substrate through electrospinning. Prior to the start of these studies, a series of RWSF concentrations (1, 3, 5, 7, wt%) were utilized to determine the optimal concentration
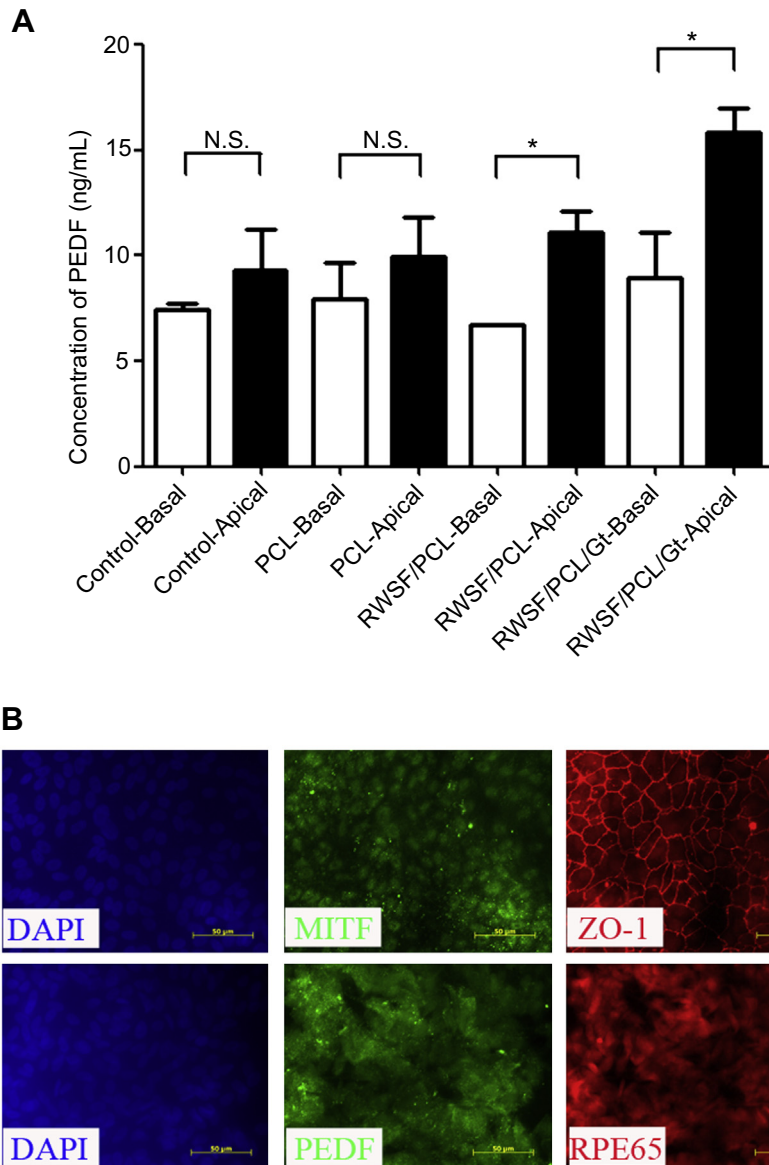
Fig. 7. ELISA analysis of PEDF secretion and immunohistochemistry of ARPE-19 cells grown on electrospun membranes for 4 weeks. (A) ARPE-19 cells only exhibited polar secretion of PEDF when they were seeded on RWSF/PCL/Gt or RWSF/PCL membranes. (B) Immunohistochemical staining demonstrated that ARPE-19 cells cultured on RWSF/PCL/Gt membranes positively expressed MITF, ZO-1, RPE65, and PEDF. (Scale bar = 50 μm).

for cell adhesion, and 5% RWSF showed a significant improvement of cell attachment compared to the other concentrations (data not shown). The incorporation of gelatin resulted in an increase in fiber diameter and pore size that was consistent with our previous reports [12]. The decreased contact angle of RWSF/PCL/Gt (64.5 ± 4.9°) compared with RWSF/PCL (119.0 ± 6.5°) indicated increased hydrophilicity of the nanofibrous membranes, possibly due to the hydrophilic groups introduced with gelatin.
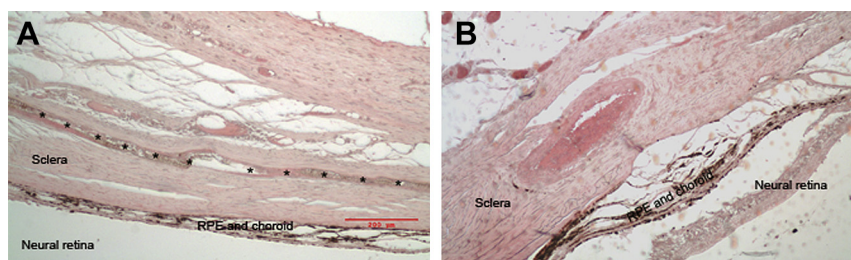
Fig. 8. Micrograph of hematoxylin and eosin (HE) stained sections of substrates implanted into rabbit eye 1-month after surgery. (A) RWSF/PCL/Gt membranes (marked with black asterisks) placed into the sclera did not show obvious inflammatory responses, and no evidence of degradation was observed. (B) Control eye without implants. Scale bar: 200 μm.

Adequate pores in a prosthetic substrate are required to allow permeability of oxygen and the movement of nutrients and metabolic waste [50]. In our studies, all of the nanofibrous membranes showed proper porosity (>85%) and appropriate pore size (>680 nm) compared to previously published data [51,52]. Additionally, the thickness of Bruch's membrane changes with aging, which correlates with RPE function *in vivo* [53,54]; importantly our electrospun membranes can be consistently reproduced in a range of desired thicknesses, comparable to the native Bruch's membrane at different ages, simply by regulating the electrospun parameters (e.g. processing time).

Generally, RPE cell survival post-transplantation is limited because of poor attachment of the transplanted cells to the pathological Bruch's membrane, leading to failure of RPE transplantation [55]. Proteins containing RGD tripeptides, together with integrins that mediate cell attachment are widely used to promote cell adhesion [56]. Similarly, incorporation of gelatin into hydrophobic polymers can have an additional effect [57]. Consequently, in our studies, ARPE-19 cell attachment was significantly enhanced by addition of the RGD-rich RWSF and gelatin.

Following the same period of incubation, RPE cell viability on the various nanofibrous membranes was compared using the WST-1 assay. This is a test based on the intact activity of cellular mitochondrial dehydrogenases, and it is widely used for non-radioactive quantification of cell proliferation and viability. Our results confirmed that ARPE-19 cells grow on PCL, RWSF/PCL and RWSF/PCL/Gt membranes, albeit initially there was no statistical differences among these artificial Bruch's membranes ($p > 0.05$). However, with prolonged incubation, ARPE-19 cells showed the highest viability on RWSF/PCL/Gt membranes, followed by RWSF/PCL membranes, and then by PCL membranes, possibly due to the incorporation of RGD peptides and to the consequent improvement of hydrophilicity, as suggested by others' reports [23,58].

We conducted flow cytometric analysis to examine the cell cycle in order to compare the proliferation indices of ARPE-19 cells cultured on the different artificial Bruch's membranes. Our results confirmed that RWSF can significantly drive more cells into active cycling (G2/M + S) than pure PCL. Moreover, the highest proliferation index was observed when ARPE-19 cells were seeded on RWSF/PCL/Gt membranes, which suggests that cytocompatibility can be further improved by gelatin.

It has been reported that RPE cells frequently change their epithelial phenotype to mesenchymal-like cells under some conditions, which is defined as epithelial mesenchymal transition (EMT). After EMT, RPE cells lose many of the RPE-specific characteristics, including expression of key genes. Additionally, according to Theisen's results, gene expression in human cells can also be altered by nanofibers [59]. We tested for the expression of 9 marker genes, and ARPE-19 cells cultured on the different membranes showed equivalent levels of expression to those cultured on TCP, suggesting that our electrospun membranes did not disturb normal RPE-cell gene expression. More importantly, RNA-sequencing result clearly demonstrated that primary RPE-EMs complex expresses similar signature genes compared with the primary RPE cells from an identical source. These data strongly suggested that our unique membranes did not alter the molecular signatures of RPE cells.

Few previous publications examined whether their artificial Bruch's membranes altered the secretion of pro-inflammatory factors by RPE cells. *IL-6* is a pro-inflammatory cytokine that is associated with the occurrence of intraocular inflammatory diseases [60]. *MCP-1* and *IL-1β* are considered to be the key genes to mediate monocyte infiltration and immunocompetent cell migration during inflammatory retinal diseases [61,62]. Fortunately, we observed that long-term culture of ARPE-19 cells on all types of electrospun membranes did not increase the expression of *MCP-1, IL-1β* and *IL-6* compared to TCP culture conditions.

PEDF, a secreted factor characteristic of RPE cells, has the key neurotrophic function and, importantly, it also inhibits retinal and choroidal neovascularization [63]. Additionally, PEDF expression is also used as an important criterion to evaluate the functionality of polarized RPE cells [42]. Based on our studies, ARPE-19 cells only exhibited polar secretion of PEDF when seeded on RWSF/PCL/Gt and RWSF/PCL membranes after 4 weeks of culture. Furthermore, ARPE-19 seeded on RWSF/PCL/Gt membranes expressed notably higher PEDF levels than cells growing on RWSF/PCL membranes, and this result may be due to the formation of more polarized RPE cells. Overall, these results suggest that both RWSF/PCL/Gt and RWSF/PCL membranes could accelerate the functionalization of RPE cells, with an enhanced effect of the former.

Pigmentation is a native RPE phenotype *in vivo*, and it is usually utilized as an important differentiation marker of RPE cells [42]. However, pigmentation has never occurred in ARPE-19 cells cultured on artificial substrates in other studies. The ARPE-19 cell line is used widely as a substitute for primary RPE cells, and the standard culture media for these cells is DMEM/F12, although cumulative evidence demonstrated that many of the RPE differentiation markers are usually lost under these conditions. As reported by Shadforth's studies, ARPE-19 cells can restore some of their phenotypes such as the formation of tight junctions and microvilli-like structures, as well as positive expression of some RPE-specific proteins when cultured in medium containing 1% FBS for more than 7 weeks on *Bombyx m*ori silk fibroin prosthetic Bruch's membranes [21]. Nevertheless, pigmentation was not observed in this study. Unprecedentedly, ARPE-19 cells cultured on our RWSF/PCL/Gt membranes for 90 days showed perceptible pigmented areas indicating that our culture systems are feasible for differentiation of RPE cells.

ARPE-19 cells cultured on RWSF/PCL/Gt membranes for 30 days were viewed using SEM. Encouragingly, ARPE-19 seeded on RWSF/PCL/Gt membranes grew well and formed a confluent monolayer of cells consisting of a polygonal morphology with tight junctions. Furthermore, microvilli-like structures were also observed on the apical surfaces of ARPE-19 cells. According to previous reports, ARPE-19 cells rarely exhibit this morphologic characteristic under routine culture conditions [42]. Our results suggest that long-term co-cultures established on RWSF/PCL/Gt membranes maintained this development potential and also induced RPE-like cellular extensions.

Immunohistochemical staining has shown that ARPE-19 cells cultured on RWSF/PCL/Gt membranes strongly expressed MITF, a regulator for RPE cell differentiation and proliferation, and formed mature cell–cell junctions and hexagonal shapes confirmed by positive expression of ZO-1. Further, these cells also expressed RPE65, an RPE-specific enzyme essential for retinoid recycling, and PEDF, a neurotrophic factor that acts to stabilize the neuronal retina, suggesting that RWSF/PCL/Gt membranes not only promote the long-term viability of ARPE-19 cells, but also enhance various differentiated features of functional RPE cells during long-term co-culture [42]. One of these features is the ability for phagocytosis, which is used to clear POS from the apical side *in vivo*. ARPE-19 cells cultured on RWSF/PCL/Gt membranes exhibited phagocytic capabilities for porcine POS, which is in agreement with the presence of microvilli as showed in Fig. 6.

According to previous studies, some researchers transplanted their artificial RPE substrates into different site of animal eyes, such as subconjunctival and subretina [19].In our investigations, the RWSF/PCL/Gt membrane was implanted into sclera for primary evaluation of biocompability *in vivo* due to its easy-operation. Additionally, we used RWSF/PCL/Gt membrane without human

RPE cells for animal tests in order to prevent any inflammatory response, comparable to the results confirmed by Rezai and his colleagues after transplantation of human fetal RPE cells seeded to a PLG polymer film into the rabbit eye [64].

5. Conclusion

Novel Bruch's membrane-mimetic substrates with high porosity and similar thickness to native Bruch's membranes were prepared from RWSF, PCL, Gt with weight ratio of 5:85:10 via electrospinning. We confirmed the feasibility of using these electrospun membranes as alternatives to Bruch's membrane for long-term sustainable culture and growth of functional RPE cells. We found that RWSF/PCL/Gt membranes not only accelerated RPE cell growth and proliferation without any inflammatory reaction, but also promoted the functionalization of RPE cells. Electrospun RWSF/PCL/Gt membranes are therefore appropriate candidates for exploration as a carrier for RPE transplantation.

Acknowledgments

Appendix A. Supplementary data

Supplementary data related to this article can be found online at http://dx.doi.org/10.1016/j.biomaterials.2014.08.040.

References

[1] Strauss O. The retinal pigment epithelium in visual function. Physiol Rev 2005;85:845—81.
[2] Kokkinaki M, Sahibzada N, Golestaneh N. Human induced pluripotent stem-derived retinal pigment epithelium (RPE) cells exhibit ion transport, membrane potential, polarized vascular endothelial growth factor secretion, and gene expression pattern similar to native RPE. Stem Cells 2011;29:825—35.
[3] Ming M, Li X, Fan X, Yang D, Li L, Chen S, et al. Retinal pigment epithelial cells secrete neurotrophic factors and synthesize dopamine: possible contribution to therapeutic effects of RPE cell transplantation in Parkinson's disease. J Transl Med 2009;7:53.
[4] Zhu D, Deng X, Spee C, Sonoda S, Hsieh CL, Barron E, et al. Polarized secretion of PEDF from human embryonic stem cell-derived RPE promotes retinal progenitor cell survival. Invest Ophthalmol Vis Sci 2011;52:1573—85.
[5] Rowland TJ, Buchholz DE, Clegg DO. Pluripotent human stem cells for the treatment of retinal disease. J Cell Physiol 2012;227:457—66.
[6] Wang H, Yagi F, Cheewatrakoolpong N, Sugino IK, Zarbin MA. Short-term study of retinal pigment epithelium sheet transplants onto Bruch's membrane. Exp Eye Res 2004;78:53—65.
[7] Seiler MJ, Aramant RB. Cell replacement and visual restoration by retinal sheet transplants. Prog Retin Eye Res 2012;31:661—87.
[8] Lewallen M, Xie T. Cell-based therapies for retinal degenerative diseases: a thousand strategies. J Glaucoma 2013;22(Suppl. 5):S42—5.
[9] da Cruz L, Chen FK, Ahmado A, Greenwood J, Coffey P. RPE transplantation and its role in retinal disease. Prog Retin Eye Res 2007;26:598—635.
[10] Lamba DA, Karl MO, Reh TA. Strategies for retinal repair: cell replacement and regeneration. Prog Brain Res 2009;175:23—31.
[11] Gouras P, Kong J, Tsang SH. Retinal degeneration and RPE transplantation in Rpe65(-/-) mice. Invest Ophthalmol Vis Sci 2002;43:3307—11.
[12] Xiang P, Li M, Zhang C-y, Chen D-l, Zhou Z-h. Cytocompatibility of electrospun nanofiber tubular scaffolds for small diameter tissue engineering blood vessels. Int J Biol Macromol 2011;49:281—8.
[13] Li Y, Tsai YT, Hsu CW, Erol D, Yang J, Wu WH, et al. Long-term safety and efficacy of human-induced pluripotent stem cell (iPS) grafts in a preclinical model of retinitis pigmentosa. Mol Med 2012;18:1312—9.
[14] Engelhardt M, Tosha C, Lopes VS, Chen B, Nguyen L, Nusinowitz S, et al. Functional and morphological analysis of the subretinal injection of retinal pigment epithelium cells. Vis Neurosci 2012;29:83—93.

[15] Schwartz SD, Hubschman J-P, Heilwell G, Franco-Cardenas V, Pan CK, Ostrick RM, et al. Embryonic stem cell trials for macular degeneration: a preliminary report. Lancet;379:713—720.
[16] Tezel TH, Del Priore LV, Berger AS, Kaplan HJ. Adult retinal pigment epithelial transplantation in exudative age-related macular degeneration. Am J Ophthalmol 2007;143:584—95.
[17] Del Priore LV, Kaplan HJ, Tezel TH, Hayashi N, Berger AS, Green WR. Retinal pigment epithelial cell transplantation after subfoveal membranectomy in age-related macular degeneration: clinicopathologic correlation. Am J Ophthalmol 2001;131:472—80.
[18] Lu JT, Lee CJ, Bent SF, Fishman HA, Sabelman EE. Thin collagen film scaffolds for retinal epithelial cell culture. Biomaterials 2007;28:1486—94.
[19] Thumann G, Viethen A, Gaebler A, Walter P, Kaempf S, Johnen S, et al. The in vitro and in vivo behaviour of retinal pigment epithelial cells cultured on ultrathin collagen membranes. Biomaterials 2009;30:287—94.
[20] Thumann G, Hueber A, Dinslage S, Schaefer F, Yasukawa T, Kirchhof B, et al. Characteristics of iris and retinal pigment epithelial cells cultured on collagen type I membranes. Curr Eye Res 2006;31:241—9.
[21] Shadforth AM, George KA, Kwan AS, Chirila TV, Harkin DG. The cultivation of human retinal pigment epithelial cells on Bombyx mori silk fibroin. Biomaterials 2012;33:4110—7.
[22] Subrizi A, Hiidenmaa H, Ilmarinen T, Nymark S, Dubruel P, Uusitalo H, et al. Generation of hESC-derived retinal pigment epithelium on biopolymer coated polyimide membranes. Biomaterials 2012;33:8047—54.
[23] Tezcaner A, Bugra K, Hasirci V. Retinal pigment epithelium cell culture on surface modified poly(hydroxybutyrate-co-hydroxyvalerate) thin films. Biomaterials 2003;24:4573—83.
[24] Thomson HA, Treharne AJ, Walker P, Grossel MC, Lotery AJ. Optimisation of polymer scaffolds for retinal pigment epithelium (RPE) cell transplantation. Br J Ophthalmol 2011;95:563—8.
[25] Williams R, Krishna Y, Dixon S, Haridas A, Grierson I, Sheridan C. Polyurethanes as potential substrates for sub-retinal retinal pigment epithelial cell transplantation. J Mater Sci Mater Med 2005;16:1087—92.
[26] Harkin DG, George KA, Madden PW, Schwab IR, Hutmacher DW, Chirila TV. Silk fibroin in ocular tissue reconstruction. Biomaterials 2011;32:2445—58.
[27] Ito A, Hibino E, Kobayashi C, Terasaki H, Kagami H, Ueda M, et al. Construction and delivery of tissue-engineered human retinal pigment epithelial cell sheets, using magnetite nanoparticles and magnetic force. Tissue Eng 2005;11:489—96.
[28] Treharne AJ, Grossel MC, Lotery AJ, Thomson HA. The chemistry of retinal transplantation: the influence of polymer scaffold properties on retinal cell adhesion and control. Br J Ophthalmol 2011;95:768—73.
[29] Dong Y, Yong T, Liao S, Chan CK, Stevens MM, Ramakrishna S. Distinctive degradation behaviors of electrospun polyglycolide, poly(DL-lactide-co-glycolide), and poly(L-lactide-co-epsilon-caprolactone) nanofibers cultured with/without porcine smooth muscle cells. Tissue Eng Part A 2010;16:283—98.
[30] Chen H, Fan X, Xia J, Chen P, Zhou X, Huang J, et al. Electrospun chitosan-graft-poly (varepsilon-caprolactone)/poly (varepsilon-caprolactone) nanofibrous scaffolds for retinal tissue engineering. Int J Nanomedicine 2011;6:453—61.
[31] Fon D, Zhou K, Ercole F, Fehr F, Marchesan S, Minter MR, et al. Nanofibrous scaffolds releasing a small molecule BDNF-mimetic for the re-direction of endogenous neuroblast migration in the brain. Biomaterials 2014;35:2692—712.
[32] Zhao W, Ju YM, Christ G, Atala A, Yoo JJ, Lee SJ. Diaphragmatic muscle reconstruction with an aligned electrospun poly(ε-caprolactone)/collagen hybrid scaffold. Biomaterials 2013;34:8235—40.
[33] Lee J, Yoo JJ, Atala A, Lee SJ. The effect of controlled release of PDGF-BB from heparin-conjugated electrospun PCL/gelatin scaffolds on cellular bioactivity and infiltration. Biomaterials 2012;33:6709—20.
[34] Woodruff MA, Hutmacher DW. The return of a forgotten polymer—polycaprolactone in the 21st century. Prog Polym Sci 2010;35:1217—56.
[35] Christiansen AT, Tao SL, Smith M, Wnek GE, Prause JU, Young MJ, et al. Subretinal implantation of electrospun, short nanowire, and smooth poly(epsilon-caprolactone) scaffolds to the subretinal space of porcine eyes. Stem Cells Int 2012;2012:454295.
[36] Cai S, Smith ME, Redenti SM, Wnek GE, Young MJ. Mouse retinal progenitor cell dynamics on electrospun poly(varepsilon-caprolactone). J Biomater Sci Polym Ed 2011;23:1451—65.
[37] Pritchard CD, Arner KM, Langer RS, Ghosh FK. Retinal transplantation using surface modified poly(glycerol-co-sebacic acid) membranes. Biomaterials 2010;31:7978—84.
[38] Li X, Zhang C, Wang L, Ma C, Yang W, Li M. Acylation modification of antheraea pernyi silk fibroin using succinic anhydride and its effects on enzymatic degradation behavior. J Chem 2013;2013. 640913.
[39] Ruoslahti E. RGD and other recognition sequences for integrins. Annu Rev Cell Dev Biol 1996;12:697—715.
[40] Wu L, Li M, Zhao J, Chen D, Zhou Z. Preliminary study on polyvinyl alcohol/wild antheraea pernyi silk fibroin as nanofiber scaffolds for tissue engineered tendon. Zhongguo xiu fu chong jian wai ke za zhi = Zhongguo xiufu chongjian waike zazhi = Chin J Reparative Reconstr Surg 2011;25:181—6.
[41] Sonoda S, Spee C, Barron E, Ryan SJ, Kannan R, Hinton DR. A protocol for the culture and differentiation of highly polarized human retinal pigment epithelial cells. Nat Protoc 2009;4:662—73.

[42] Ahmado A, Carr AJ, Vugler AA, Semo M, Gias C, Lawrence JM, et al. Induction of differentiation by pyruvate and DMEM in the human retinal pigment epithelium cell line ARPE-19. Invest Ophthalmol Vis Sci 2011;52:7148–59.

[43] Finnemann SC, Bonilha VL, Marmorstein AD, Rodriguez-Boulan E. Phagocytosis of rod outer segments by retinal pigment epithelial cells requires αvβ5 integrin for binding but not for internalization. Proc Natl Acad Sci 1997;94:12932–7.

[44] Liu Z, Yu N, Holz FG, Yang F, Stanzel BV. Enhancement of retinal pigment epithelial culture characteristics and subretinal space tolerance of scaffolds with 200 nm fiber topography. Biomaterials 2014;35:2837–50.

[45] Liao J-L, Yu J, Huang K, Hu J, Diemer T, Ma Z, et al. Molecular signature of primary retinal pigment epithelium and stem-cell-derived RPE cells. Hum Mol Genet 2010;19:4229–38.

[46] Kevany BM, Palczewski K. Phagocytosis of retinal rod and cone photoreceptors. Physiology 2010;25:8–15.

[47] Gonzalez-Cordero A, West EL, Pearson RA, Duran Y, Carvalho LS, Chu CJ, et al. Photoreceptor precursors derived from three-dimensional embryonic stem cell cultures integrate and mature within adult degenerate retina. Nat Biotechnol 2013;31:741–7.

[48] Treharne AJ, Thomson HAJ, Grossel MC, Lotery AJ. Developing methacrylate-based copolymers as an artificial Bruch's membrane substitute. J Biomed Mater Res Part A 2012;100A:2358–64.

[49] Binder S. Scaffolds for retinal pigment epithelium (RPE) replacement therapy. Br J Ophthalmol 2011;95:441–2.

[50] Rodrigues MT, Martins A, Dias IR, Viegas CA, Neves NM, Gomes ME, et al. Synergistic effect of scaffold composition and dynamic culturing environment in multilayered systems for bone tissue engineering. J Tissue Eng Regen Med 2012;6:e24–30.

[51] Booij JC, Baas DC, Beisekeeva J, Gorgels TG, Bergen AA. The dynamic nature of Bruch's membrane. Prog Retin Eye Res 2010;29:1–18.

[52] Heth CA, Yankauckas MA, Adamian M, Edwards RB. Characterization of retinal pigment epithelial cells cultured on microporous filters. Curr Eye Res 1987;6: 1007–19.

[53] Curcio CA, Johnson M. Structure, function, and pathology of Bruch's membrane. Elastic 2012;146:210–3.

[54] Karampelas M, Sim DA, Keane PA, Papastefanou VP, Sadda SR, Tufail A, et al. Evaluation of retinal pigment epithelium-Bruch's membrane complex thickness in dry age-related macular degeneration using optical coherence tomography. Br J Ophthalmol 2013;97:1256–61.

[55] Afshari F, Fawcett J. Improving RPE adhesion to Bruch's membrane. Eye 2009;23:1890–3.

[56] Hersel U, Dahmen C, Kessler H. RGD modified polymers: biomaterials for stimulated cell adhesion and beyond. Biomaterials 2003;24:4385–415.

[57] Ma Z, He W, Yong T, Ramakrishna S. Grafting of gelatin on electrospun poly (caprolactone) nanofibers to improve endothelial cell spreading and proliferation and to control cell orientation. Tissue Eng 2005;11:1149–58.

[58] Singh AK, Srivastava GK, Martin L, Alonso M, Pastor JC. Bioactive substrates for human retinal pigment epithelial cell growth from elastin-like recombinamers. J Biomed Mater Res Part A 2014;102:639–46.

[59] Theisen C, Fuchs-Winkelmann S, Knappstein K, Efe T, Schmitt J, Paletta J, et al. Influence of nanofibers on growth and gene expression of human tendon derived fibroblast. Biomed Eng OnLine 2010;9:1–12.

[60] Ishihara K, Hirano T. IL-6 in autoimmune disease and chronic inflammatory proliferative disease. Cytokine Growth Factor Rev 2002;13:357–68.

[61] Nakazawa T, Hisatomi T, Nakazawa C, Noda K, Maruyama K, She H, et al. Monocyte chemoattractant protein 1 mediates retinal detachment-induced photoreceptor apoptosis. Proc Natl Acad Sci U S A 2007;104:2425–30.

[62] Liu Y, Yang X, Utheim TP, Guo C, Xiao M, Liu Y, et al. Correlation of cytokine levels and microglial cell infiltration during retinal degeneration in RCS rats. PLoS One 2013;8:e82061.

[63] Tombran-Tink J, Barnstable CJ. PEDF: a multifaceted neurotrophic factor. Nat Rev Neurosci 2003;4:628–36.

[64] Rezai KA, Farrokh-Siar L, Godowski K, Patel SC, Ernest JT. A model for xenogenic immune response. Graefe's Archive Clin Exp Ophthalmol 2000;238: 352–8.